Ion Acceleration by Collisionless Shocks in High-Intensity-Laser–Underdense-Plasma Interaction

M. S. Wei,[1] S. P. D. Mangles,[1] Z. Najmudin,[1] B. Walton,[1] A. Gopal,[1] M. Tatarakis,[1,*] A. E. Dangor,[1] E. L. Clark,[1,2] R. G. Evans,[1,2] S. Fritzler,[3] R. J. Clarke,[4] C. Hernandez-Gomez,[4] D. Neely,[4] W. Mori,[5] M. Tzoufras,[5] and K. Krushelnick[1]

[1]*Blackett Laboratory, Imperial College, London, SW7 2BZ, United Kingdom*
[2]*Plasma Physics Department, Atomic Weapons Establishment plc, Aldermaston, Reading RG7 4PR, United Kingdom*
[3]*Laboratoire d'Optique Appliquée, École Polytechnique, ENSTA, Palaiseau, France*
[4]*Central Laser Facility, Rutherford Appleton Laboratory, Chilton, Oxon, OX11 0QX, United Kingdom*
[5]*Department of Physics and Astronomy and of Electrical Engineering, UCLA, Los Angeles, California 90095, USA*

(Received 24 February 2004; published 7 October 2004)

Ion acceleration by the interaction of an ultraintense short-pulse laser with an underdense-plasma has been studied at intensities up to 3×10^{20} W/cm^2. Helium ions having a maximum energy of 13.2 ± 1.0 MeV were measured at an angle of 100° from the laser propagation direction. The maximum ion energy scaled with plasma density as $n_e^{0.70\pm0.05}$. Two-dimensional particle-in-cell simulations suggest that multiple collisionless shocks are formed at high density. The interaction of shocks is responsible for the observed plateau structure in the ion spectrum and leads to an enhanced ion acceleration beyond that possible by the ponderomotive potential of the laser alone.

DOI: 10.1103/PhysRevLett.93.155003 PACS numbers: 52.38.Kd, 52.38.Hb, 52.65.Rr

Throughout the past decade, continuing developments in high-intensity, short-pulse laser technology have stimulated significant interest in electron acceleration using laser-produced plasmas. This is important for applications such as compact particle accelerators [1,2] and fast ignition for inertial confinement fusion [3]. In addition, ions can be accelerated by the strong space charge field generated by the transverse ponderomotive force of the laser which expels electrons from the region where the laser beam is intense [4,5]. Study of the ion dynamics is important as it can supply valuable information of the fundamental physics of the interaction of a high-intensity laser with underdense plasma, such as self-focusing and channelling due to relativistic and charge displacement effects [6–9]. It is also directly related to the observations of anomalously high yields of neutrons resulting from hot channel formation [10,11]. The maximum ion energy that can be produced by this process is roughly equal to the ponderomotive energy. Krushelnick et al. [4] have observed helium ions with peak energies of 3.6 MeV, deuterons up to 1 MeV and neon ions with energy greater than 6 MeV. From the maximum ion energy measurements, it was inferred that the peak laser intensity in the experiments was a few times the focused intensity in vacuum due to self-focusing of the high-intensity laser in plasma.

This Letter presents measurements of energetic ions accelerated during the interaction of a 0.25 PW laser with a gas-jet plasma at electron densities up to 1.4×10^{20} cm^{-3}. Thus P_L/P_c is greater than 2000, where P_L is the laser power and P_c is the critical power required for relativistic self-focusing to dominate diffraction, which is given by $P_c \sim 17.4(n_c/n_e)$ GW, where n_e is the plasma density and n_c is the critical density. The vacuum intensity of the laser was up to 3×10^{20} W/cm^2, which corresponds to a normalized vector potential $a_0 = eE/mc\omega_0 \sim 15$. Helium ions with energy up to 13.2 ± 1.0 MeV are measured in a direction of 100° from the laser axis. A strong correlation is observed between the maximum ion energy and the initial plasma density. The ion energy spectrum at high density shows a well defined plateau structure. Particle-in-cell (PIC) simulations indicate that the plateau is produced by the interaction of multiple radial electrostatic shocks produced by the transverse ponderomotive force, which act as an additional acceleration mechanism.

The experiments were performed using the VULCAN Petawatt laser beam line at the Rutherford Appleton Laboratory. For these investigations, the laser produced pulses with an energy up to 180 J in a duration of 0.5–0.7 ps at a wavelength of 1.054 μm. The laser pulse was focused onto the edge of a supersonic gas jet (2 mm nozzle diameter) using an $f/3$ off-axis parabolic mirror to a focal spot size of 10 μm in vacuum. When helium was used as the working gas, the backing pressure in the gas nozzle was varied to give a plasma density between $(0.04–1.4) \times 10^{20}$ cm^{-3}. The electron density during the interaction was obtained by measuring the plasma frequency (ω_p) from simultaneous forward Raman scattering measurements. Deuterium gas was also used but at a lower density.

The energy spectrum of the ions at 100° from the laser propagation direction was measured with a Thomson parabola ion spectrometer, which enables ions with different charge to mass ratio to be distinguished since they produce unique parabolic trajectories at the detector plane. The spectrometer was positioned 80 cm from the

interaction region. A 250 μm diameter pinhole served as the entrance to the spectrometer, subtending a solid angle of 7.67×10^{-8} steradians. The ions were recorded on a 1 mm thick piece of CR39 nuclear track detector.

The angular distribution of the ions was measured with a stack of several layers of radiochromic film (RCF) strips parallel to the direction of laser propagation placed at a distance of 6 cm radially from the interaction region. The angular distribution of ions in different energy ranges was determined through the use of aluminum filters of various thickness in front of the RCF.

Typical helium ion spectra at a high and a low plasma density are shown in Fig. 1. The spectra show two main characteristics: i) the maximum ion energy and the number of energetic ions are higher at high density; ii) at high density, a plateau is observed at high energy. In the high density case shown in Fig. 1(a), both He^{2+} and He^{1+} ions have been accelerated to high energy, the maximum energy for He^{2+} being 13.2 ± 1.0 MeV. The total number of He^{2+} ions with energy greater than 680 keV is 3.8×10^{11}. It should be noted that there is a reduction in the number of He^{2+} at energy less than 1 MeV, despite the ion energy being well above the detection threshold of CR39. This is due to the strong charge-exchange/recombination of ions with the surrounding background neutral gas as they move out of the interaction region. Since the cross section for charge exchange is greater at lower E ($\sigma \propto 1/E^3$), less energetic He^{2+} ions are more likely to recombine while passing through the neutral gas. This is confirmed by the large number of He^{1+} ions observed, despite the laser intensity being much greater than the threshold for full ionization of helium over nearly the whole extent of the laser focal volume in the gas jet. At low density [Fig. 1(b)], both the number of ions accelerated and the maximum energy are greatly reduced, even though the laser energy on this shot was marginally greater than that for Fig. 1(a). The maximum ion energy drops to 2.3 MeV and the total number of He^{2+} ions with energy greater than 590 ± 20 keV is reduced to 7.4×10^{10}. At even lower density, i.e., below 4×10^{18} cm^{-3}, no energetic helium ions (greater than 100 keV/nucleon—the detector threshold) were observed.

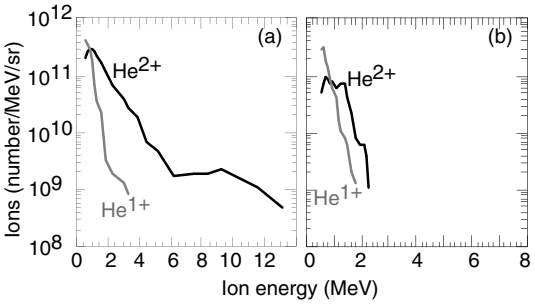

FIG. 1. Energy spectra of helium ions for (a) high density, 1.4×10^{20} cm^{-3}, and (b) low density, 1.7×10^{19} cm^{-3}.

The He^{2+} ion spectrum exhibits a plateau in the energy range between 6–10 MeV and has a cutoff at the maximum ion energy recorded on the detector. The plateau structure is a characteristic of the acceleration due to laser driven laminar shock waves [12].

Figure 2 shows a plot of maximum ion energy per nucleon against plasma density. The power law fit ($E_{max} \propto n_e^{0.70\pm0.05}$) suggests a much stronger correlation of ion acceleration with plasma density compared to that found at lower power laser underdense-plasma interaction ($E_{max} \propto n_e^{0.125}$) [5].

Figure 3 shows the ion angular emission distributions at low and high density. The ion emission at low density (1.0×10^{19} cm^{-3}) is predominantly at 90°. For energies greater than 2 MeV, there is a narrow lobe with an angular spread of less than 4° (FWHM). At higher plasma density, the angular spread is much greater. Even the high energy component ($E > 3.5$ MeV), which has a less broad angular emission, has an angular spread of 27°, and is preferentially emitted in the forward direction. Considering the viewing angle of the Thomson parabola (100° from the laser axis), it is likely that the maximum ion energy recorded in the detector is less than that produced during the interaction.

A series of two spatial but three momentum and field dimensions (2D3V) particle-in-cell simulations using the code OSIRIS [13] were performed. In the first set of simulations, the laser intensity was fixed at $I \sim 3 \times 10^{20}$ Wcm^{-2} ($a_0 \sim 15$). The density profile of the fully ionized helium plasma had a ramp with a distance of 0.6 mm to various peak values ($0.01n_c$, $0.05n_c$, and $0.14n_c$) which lasted 0.5 mm, and then ramped down to 0 in the last 0.6 mm. A linearly polarized laser beam with a Gaussian profile of duration 0.65 ps (FWHM) and a spot size of 20 μm (FWHM) diameter was focused onto the front edge of the plasma. This corresponds to a laser power of 1 PW. A moving window with size 839 μm (15928 grids) by 105 μm (1392 grids) in longitudinal (x) and transverse (y) directions, was used. There were two electrons and two ions per cell. Simulations with a laser power of 250 TW were also performed with all other

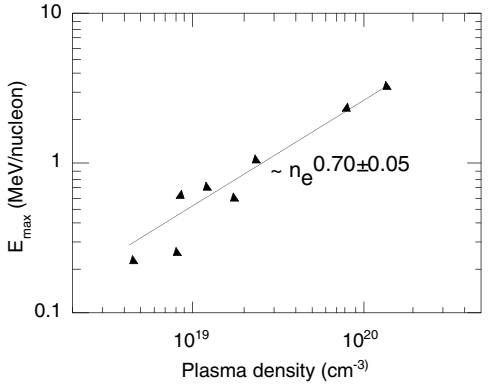

FIG. 2. Maximum ion energy (MeV per nucleon) as a function of plasma density.

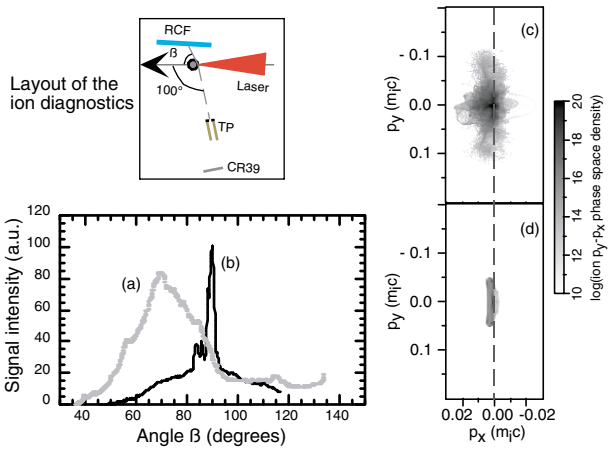

FIG. 3 (color online). Angular distribution of energetic helium ions. (a) Ions with energy greater than 3.5 MeV at high density 1.4×10^{20} cm^{-3}, (b) ions with energy greater than 2 MeV at low density 1×10^{19} cm^{-3}, (c) ion phase space p_y vs p_x plot during the shock interaction at $\tau = 2.5$ ps in the high density (1.4×10^{20} cm^{-3}) simulation and (d) for the low density simulation at the same time. The layout of the ion diagnostics is also shown.

parameters similar to the first set. In the latter case, the peak intensity was about $\sim 8 \times 10^{19}$ Wcm^{-2}, $a_0 \sim 8$.

The laser beam was observed to undergo significant self-focusing in all the simulations. The minimum width of the laser beam, due to self-focusing, was about 4 μm at $0.14 n_c$ and 8 μm at $0.01 n_c$ with $a_0 \sim 30$ and 23, respectively. The laser intensities were found to be enhanced by a factor of 4 at high density for both the 250 TW and 1 PW cases. Propagation instabilities, i.e., filamentation and beam hosing, occurred at later times.

Simulated helium ion energy spectra, which were taken at 90° with 2° acceptance angle, are presented in Fig. 4 for different densities at the same time, $\tau = 5$ ps, i.e., after the laser had propagated a distance of 1.5 mm. The spectra do not evolve significantly afterwards. The ion spectra show the same characteristics as the experimental data. The simulated maximum ion energy in the low density case is approximately equal to the ponderomotive energy, $U = Zm_e c^2(\gamma - 1)$, where $\gamma = (1 + a^2/2)^2$ is the relativistic factor of plasma electrons in the laser field. For $a_0 = 23$, U is about 15.6 MeV, c.f. the peak ion energy (12.5 MeV). At high density, the peak ion energy, ~46 MeV at 1 PW and ~20 MeV at 250 TW, is about 2 times the enhanced peak ponderomotive energy due to self-focusing. The simulations at high density reproduce the plateau structure in the ion energy spectra in both the 1 PW and 250 TW cases. The plateau is much more pronounced in the high power case. The peak ion energy in the simulations is higher than that observed in the experiments. As mentioned earlier, this is likely due to the viewing angle of our diagnostic as well as the slab geometry used in the simulations. When compared with the emission angle corresponding to that of the diagnostic, the peak energy in experiment and simulation are approximately in agreement.

From the ion momentum p_y vs p_x plots as shown in Fig. 3(c) and 3(d), it was found that ions were predominantly emitted at 90° at low density with very narrow angular spread, while, at high density, the most energetic ions were preferentially accelerated slightly forward at 90° with a much broader angular distribution as in the experiments, but different from previous measurements [4]. The peak ion energy increases with plasma density as $E_{max} \propto n_e^{0.63}$, which is again in agreement with the experiment. The enhancement of the ion acceleration and much broader angular emission at high density are observed to be due to collisonless shock acceleration observed in previous simulations [14,15].

Indeed, in the high density simulations, there are multiple electrostatic shock waves driven out radially as shown in Fig. 5. In the 250 TW simulation, where 5(a) and 5(c) show the ion phase space plot in y vs x and p_y vs x, the interactions of shocks driven by the filamented laser beam leads to the enhanced acceleration of ions. This phenomenon is much clearer in the 1 PW simulation in 5(b) and 5(d), where there are two distinct shocks appearing immediately after the laser beam self-focuses. Eventually a channel forms (70% density depletion) which has two discontinuous boundaries. The density compression in the shocks is 2–3 times the background density and the full width of the shocks is a few times c/ω_p (the collisionless skin depth). The second (faster) shock with $v_{s2} \sim 0.06c$ catches up and interacts with the first one ($v_{s1} \sim 0.03c$). The merged shock has a width greater than $10c/\omega_p$. Studying the radial momentum of the ions as a function of radial distance shows that the ions are accelerated by the interaction of the collisionless shocks.

The phase space structure in p_y vs y is identical to the structure observed in the numerical piston driven electrostatic shocks [14,16–18]: the ions reflected off the shock provide the dissipation for shock formation, while the

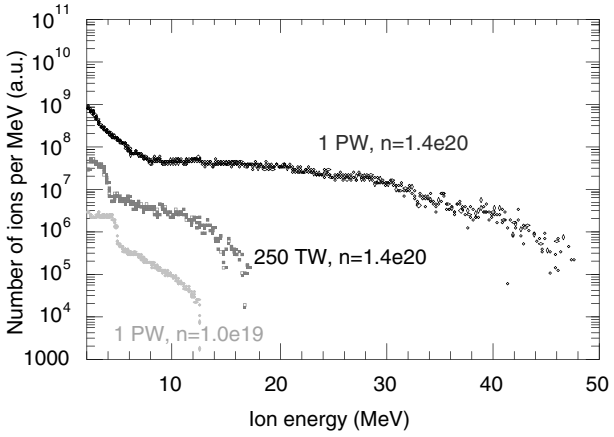

FIG. 4. Simulated ion energy spectra for different laser powers and plasma densities.

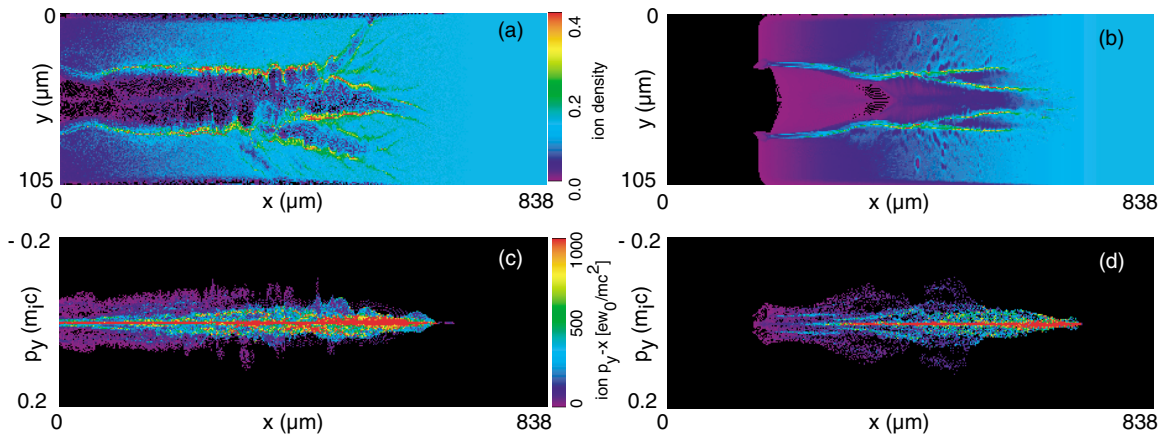

FIG. 5 (color). The ion phase space plots y vs x (a), p_y vs x (c) at $\tau = 3.1$ ps in the 250 TW case and y vs x (b), p_y vs x (d) at $\tau = 2.3$ ps in the 1 PW case from the interactions with high density plasma. Ion expulsion from the multishock interaction region is clearly shown.

ions trapped behind the shock front dissipate the wavelike structure that forms behind the shock. Large populations of ions are seen to be accelerated to higher energies especially during the merging of the multiple shocks. This is shown most clearly by an abrupt increase in the radial momentum of the ions at radial displacements well beyond the laser beam radius and thus beyond the influence of its ponderomotive force. This acceleration process contributes to the formation of the plateau in the ion energy spectrum, as has been similarly observed in other simulations at above critical density [12]. The strong dependence of the ion acceleration on plasma density can be explained by the additional shock acceleration in high density, while such mechanism does not occur in low density. The propagation angle of the second shock is often just forward of 90°, and may explain the preference of ions to be accelerated slightly in the forward direction. However, 2D simulations are likely to underestimate the influence of self-focusing, which may explain why the measured angle shift is less in simulations than in the experiment. Also, due to the degree of self-focusing, the peak intensity would be higher in 3D simulations. Therefore, the 2D PW simulations may better describe our 250 TW experiment. A full 3D simulation is still beyond the capability of present supercomputers.

In conclusion, measurements of energetic ions produced from the interaction of a short laser pulse with an underdense plasma with $P_L \gg P_c$ have been performed. A strong correlation between maximum ion energy and plasma density is evident. The observation shows that higher plasma density leads to more efficient ion acceleration. In particular, ion acceleration due to the ponderomotive expulsion of plasma is found to be enhanced by collisionless shock acceleration. The results reported here are the first experimental evidence of such acceleration in a laser plasma interaction. These results may have significance in the recent observation of anomalously high fusion yields in underdense laser-deuterium plasma interaction [11]. Furthermore, particle acceleration due to the interaction of shocks is of great importance in space and astrophysics, and consequently such interactions offer the possibility of further studying these complex processes in the laboratory.

The authors acknowledge the assistance of the staff of the Central Laser Facility of the Rutherford Appleton Laboratory in the execution of this work as well as the support of the UK Engineering and Physical Sciences Research Council (EPSRC) and the US DOE.

*Present address: Technological Educational Institute of Crete, Department of Electronics Engineering, Chania, Crete, Greece

[1] T. Tajima and J. M. Dawson, Phys. Rev. Lett. **43**, 267 (1979).
[2] V. Malka *et al.*, Science **298**, 1596 (2002).
[3] M. Tabak *et al.*, Phys. Plasmas **1**, 1626 (1994).
[4] K. Krushelnick *et al.*, Phys. Rev. Lett. **83**, 737 (1999).
[5] G. S. Sarkisov *et al.*, Phys. Rev. E **59**, 7042 (1999).
[6] G. Sun *et al.*, Phys. Fluids **30**, 526 (1987).
[7] E. Esarey and P. Sprangle, IEEE J. Quantum Electron. **33**, 1879 (1997).
[8] A. B. Borisov *et al.*, Plasma Phys. Controlled Fusion **37**, 569 (1995).
[9] Z. Najmudin *et al.*, Phys. Plasmas **10**, 438 (2003).
[10] G. Pretzler *et al.*, Phys. Rev. E **58**, 1165 (1998).
[11] S. Fritzler *et al.*, Phys. Rev. Lett. **89**, 165004 (2002).
[12] L. O. Silva *et al.*, Phys. Rev. Lett. **92**, 015002 (2004).
[13] R. Hemker, Ph.D. thesis, UCLA, 2000.
[14] W. Mori *et al.*, Phys. Rev. Lett. **60**, 1298 (1988).
[15] A. Pukhov and J. Meyer-ter-Vehn, Phys. Rev. Lett. **76**, 3975 (1996).
[16] D. W. Forslund and C. R. Shonk, Phys. Rev. Lett. **25**, 1699 (1970).
[17] D. W. Forslund and J. P. Freidberg, Phys. Rev. Lett. **27**, 1189 (1971).
[18] J. Denavit, Phys. Rev. Lett. **69**, 3052 (1992).